Doping $SrTiO_3$ supported FeSe by excess atoms and oxygen vacancies

K. V. Shanavas* and David J. Singh
Materials Science and Technology Division, Oak Ridge National Laboratory, Oak Ridge, Tennessee 37831-6056, USA
(Received 27 May 2015; published 24 July 2015)

Photoemission studies of FeSe monolayer films on $SrTiO_3$ substrate have shown electronic structures that deviate from pristine FeSe, consistent with heavy electron doping. With the help of first-principles calculations we studied the effect of excess Fe and Se atoms on the monolayer and oxygen vacancies in the substrate in order to understand the reported Fermi surface in this system. We find that both excess Fe and Se atoms prefer the same adsorption site above the bottom Se atoms on the monolayer. The adsorbed Fe is strongly magnetic and contributes electrons to the monolayer, while excess Se hybridizes with the monolayer Fe-*d* states and partially opens a gap just above the Fermi energy. We also find that the two-dimensional electron gas generated by the oxygen vacancies is partly transferred to the monolayer and can potentially suppress the hole pockets around the Γ point. Thus, both O vacancies in the $SrTiO_3$ substrate and excess Fe over the monolayer can provide high levels of electron doping.

DOI: 10.1103/PhysRevB.92.035144 PACS number(s): 74.25.Jb, 71.15.−m, 68.35.−p, 73.20.−r

I. INTRODUCTION

Superconductivity in Fe-based materials is particularly interesting in part because of its interplay with magnetism [1–5] and simple systems such as FeSe and $FeSe_{1-x}Te_x$ have attracted significant attention in recent years [6,7]. The bulk form of FeSe has a superconducting transition temperature (T_c) of 8 K, which can be enhanced up to 37 K with pressure [7–9]. Experimental measurements on single-layer FeSe films grown over $SrTiO_3$ (STO) substrate show that the samples that are metallic at room temperature open a gap of 15–20 meV when cooled, which has been attributed to a possible onset of superconductivity in this system [10–15]. The transition is reported to be above $T_c = 65$ K, with gaps of 15–20 meV. Interestingly, the effect is not observed in double layers or more [16], in contrast to FeSe films on graphene, where a transition at 2.2 K was reported on 30-nm-thick samples [17]. This has led to the speculation that the interface plays a crucial role in the properties of monolayer FeSe [18].

Photoelectron spectroscopy measurements showed that, unlike other Fe-based superconductors, the Fermi surface of single-layer FeSe on STO consists only of electron pockets at the zone corners, without hole pockets around the zone center [11]. This means that the sign-changing *s*-wave pairing state from spin fluctuation exchange in Fe-based superconductors cannot exist here and points to a different mechanism of gap opening [5]. Interestingly, measurements on samples with different annealing showed that as-prepared samples do have hole pockets around the Γ point but remain metallic to low temperatures [19]. Annealing in vacuum removes the hole pockets and also leads to the transition. Electron doping was suggested as a possible cause of the transition [19–22], which could arise from Se or O vacancies during the annealing process. However, theoretical studies showed that Se vacancies in this system lead to hole doping [23]. Scanning tunneling spectroscopy measurements on films grown on pure STO substrate find the as-prepared samples to be semiconducting and to contain excess Se [24]. Oxygen vacancies have been known to induce highly mobile two-dimensional (2D) electron gas at the polar interfaces involving STO [25].

Here, we study the effect of excess Fe and Se on the monolayer as well as oxygen vacancies in the substrate, in order to understand the observed Fermi surface of 1 unit cell FeSe on STO. We find that the excess atoms prefer a site directly above the bottom Se atoms in the FeSe monolayer, similarly to excess Fe in bulk FeTe, and that the excess Fe contributes electrons to the monolayer Fe-*d* states that may suppress the hole pockets observed around the Γ point. Excess Se, on the other hand, contributes *p* states that hybridize strongly with the monolayer Fe and lead to significant changes in the band dispersion around the Fermi level. It also suppresses the hole pockets but, at the same time, shrinks the electron pockets and induces a pseudogap just above the Fermi level. The 2D electron gas (2DEG) formed at the STO surface due to oxygen vacancies can lead to an effective attraction between STO and FeSe, also leading to electron doping in the monolayer.

II. METHODS

To study monolayer FeSe on an STO (001) surface, we used a symmetric TiO_2 terminated slab, 5.5 unit cells long, along the *c* axis separated by a vacuum layer of ∼20 Å. To accommodate the striped antiferromagnetic structure, the unit cell is enlarged to be $\sqrt{2}a \times \sqrt{2}a$ parallel to the surface. The FeSe monolayers are then added to both the top and the bottom surfaces of the slab to preserve symmetry and half of this unit cell is shown in Fig. 1. The structure is then optimized with spin polarization, allowing the *z* coordinates of the atoms to vary. The necessity of including magnetism in standard density functional structure optimizations of Fe-based superconductors is well established and has been associated with the unusual magnetic character of these compounds [3]. We tested the convergence of structural parameters with a 7.5-unit-cell STO slab and found them to be similar.

In our calculations we consider 25% doping with excess atoms, which correspond to $FeSeX_{0.25}$ where X = Fe, Se. As shown in Fig. 1, there are three sites where the excess atoms can potentially bind with FeSe. Site X_1 corresponds to one directly

*kavungalvees@ornl.gov

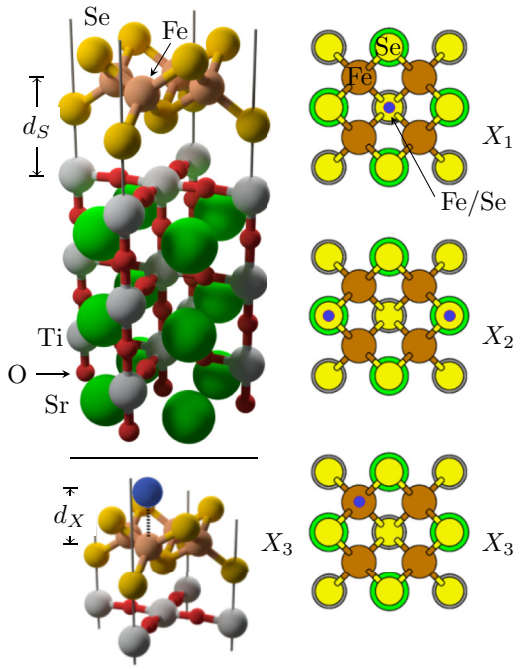

FIG. 1. (Color online) Left: Half the unit cell of monolayer FeSe on $SrTiO_3$ used in the calculations. Right: Top views of the unit cell indicating the three binding sites for excess Fe/Se atoms by blue circles. The side view of the X_3 configuration is shown at bottom left. Distances are defined as $d_S = z_{\rm Ti} - z_{\rm Fe}$ and $d_X = z_X - z_{\rm Fe}$, where z_i are the z coordinate of the atom i.

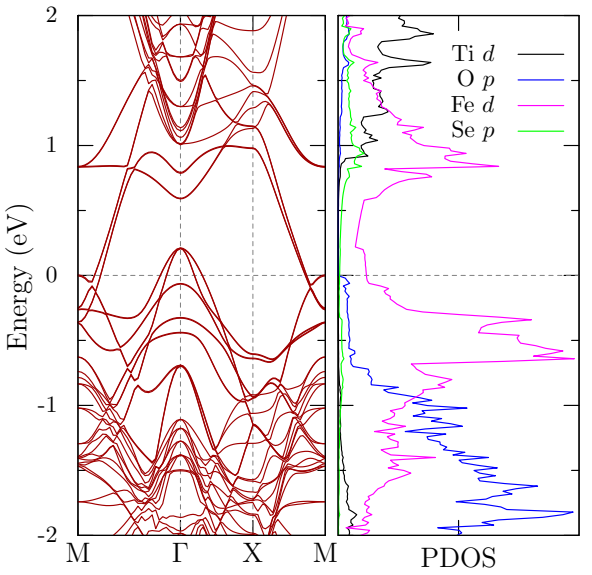

FIG. 2. (Color online) Nonmagnetic electronic band structure and partial density of states (PDOS) for the optimized structure of STO + FeSe with van der Waals interactions. Bands around the Fermi level have a strong Fe-d character and exhibit hole pockets around Γ and electron pockets around M points.

above the bottom Se atom of the monolayer as indicated by the blue circle. Site X_2 lies above one of the two Se atoms at the top of the FeSe monolayer, while X_3 corresponds to a site above Fe. The surface-to-monolayer distance is measured as the distance along the z axis between Fe and Ti ions, $d_S = z_{\rm Fe} - z_{\rm Ti}$, and the monolayer–to–excess atom distance is defined as $d_X = z_X - z_{\rm Fe}$. Finally, to simulate the 2DEG at the STO surface that arises because of oxygen vacancies we replace oxygen atoms at the STO surface partially with F using the virtual crystal approximation. Since F atoms have one more electron than O, replacing the latter with $O_{1-x}F_x$ leads to $2x$ electrons per surface unit cell. These electrons are confined close to the surface along z but have large dispersion in the in-plane directions.

All electronic structure calculations are carried out within the density functional theory as implemented in VASP code [26] using projector augmented waves [27] and the generalized gradient approximation [28] with Perdew-Burke-Ernzerhof parametrization. The kinetic energy cutoff for the plane-wave basis is taken to be 450 eV and an $11 \times 11 \times 1$ Monkhorst-Pack grid is used for reciprocal space sampling. The van der Waals (vdW) interaction is explicitly included in the calculation employing the method developed by Grimme [29] to properly describe the attraction between the substrate and the monolayers. Structural relaxations are carried out till forces are less than 0.02 eV/Å.

III. RESULTS

The in-plane lattice parameters of the supercell are set to 5.52 Å, the relaxed bulk lattice constant of STO. Full ionic relaxations are then performed keeping the cell dimensions fixed and with the striped antiferromagnetic phase for Fe moments, which is the ground state for this system [30]. We find that including the vdW interaction leads an effective attraction between the surface and the monolayer and reduces the surface Ti–to–monolayer Fe distance (d_S in Fig. 1) from 4.44 to 4.19 Å, which corresponds to a Ti-Se distance of 2.91 Å. The final structure is then used to calculate the nonmagnetic band structure and partial density of states (PDOS) shown in Fig. 2.

The valence states from the substrate have an O-p character and lie below −0.8 eV, while the conduction states are above 1 eV and are made of Ti-t_{2g} as can be seen from the PDOS in Fig. 2. Thus, the Fermi energy of the composite STO + FeSe system lie about midway in the substrate band gap and the electronic structure around the Fermi energy is from the FeSe. The Fe-d bands cross the Fermi level and form hole pockets around the Γ point and electron pockets around M points, similarly to bulk FeSe [31].

The electronic density of states (DOS) at the Fermi level is $N(E_F) = 1.24$ eV^{-1} per Fe atom and is distributed between the electron and the hole states. In Fig. 2, we can clearly see the step-like features in the Fe-d PDOS that indicate the 2D character of the band structure. From the spin-polarized calculation we get a magnetic moment of 2.4 μ_B per Fe. The Se-p states lie between −3 and −5 eV and exhibit strong covalent coupling with Fe-d orbitals.

A. Excess Fe and Se on FeSe

Next, excess Fe and Se atoms are added at the sites shown in Fig. 1 and the structures are fully relaxed within the striped antiferromagnetic order in separate calculations. Results are summarized in Table I. Surprisingly, the same site, X_1, is

TABLE I. Calculated energy differences, atomic distances, and magnetic moments of the Fe atoms of the monolayer for the STO + FeSe system with excess Fe and Se atoms. Structures are optimized in the striped antiferromagnetic phase.

	Bare	Fe_1	Fe_2	Fe_3	Se_1	Se_2	Se_3
$E - E_0$ (eV/f.u.)	–	0.00	0.71	0.42	0.00	0.17	0.28
d_S (Å)	4.19	4.28	4.22	4.29	4.29	4.25	4.15
d_X (Å)	–	1.51	3.43	2.55	1.60	3.62	2.87
m_{Fe} (μ_B)	2.38	2.26	2.11	2.30	1.82	2.09	1.29

found to have the lowest energy for both excess anion and excess cation adsorption. This site is neither a good cation site nor a good anion site but, rather, favors more covalent bonding, as previously noted in the case of FeTe. This leads to the unusual monovalent state of excess Fe [32]. This site also allows the closest distances between excess atoms and the monolayer, with $d_X = 1.51$ and 1.60 Å for Fe and Se, respectively. As reported in Table I, the magnetic moments of the iron atoms in the monolayer diminish from the bare values upon doping. The reduction is larger for Se doping; in the case of Se_1, the average Fe moments are 1.82 μ_B, reduced from 2.38 μ_B. The excess Fe is found to be strongly magnetic, with moments of 2.8, 3.1, and 2.6 μ_B for Fe_1, Fe_2, and Fe_3 respectively, consistent with excess Fe calculations on bulk FeTe [32].

Consistent with previous calculations, [23] we find that Se doping removes the electrons from the Fe-d orbitals, evidence of which can be seen from the PDOS plots in Fig. 3. The partial Fe-d DOS for FeSe + Se_1 is shifted upward compared to the same plot in Fig. 2. As a consequence, the Fe moments are reduced substantially, as reported in Table I, upon Se doping. On the other hand, Fe_1 donates electrons to the monolayer, shifting the Fe-d bands lower. For the Fe doped electronic structure plots in Fig. 3, the excess Fe is allowed to be spin-polarized while the other atoms have close to zero moment. This was done to keep the correct number of electrons in the monolayer.

Dispersion of the Fe bands is modified by the presence of excess atoms on the monolayer. In the case of Fe_1, the Fe-d bands are shifted downward, which removes the hole pockets and makes the electron pockets deeper as shown in Fig. 2. The effect of excess Se is more pronounced; overlap of Se-p orbitals with Fe-d changes the shape of the electron and hole pockets. A new hole pocket appears around the X point in the new Brillouin zone, while the electron pocket around Γ (or around M in the smaller unit cell) shrinks in size. Also, the DOS drops to almost 0, opening a pseudogap of ∼0.15 eV just above the Fermi level in the Se doped case.

The effect of excess atoms on the monolayer Fe DOS is shown in Fig. 4. In the case of excess Fe, the Fe_1-d states lie −2 eV below the Fermi level and shifts the monolayer Fe-d states to lower energies via electron doping. The Se_1-p states, on the other hand, have large dispersion and overlap with Fe-d across a wide range. This leads to rearrangement of the Fe-d states and the observed depletion of density just above the Fermi level.

B. Oxygen vacancies in STO

Bare STO surfaces with TiO_2 termination are known to develop a 2D electron gas which is localized to within a few unit cells. It is believed to originate from oxygen vacancies at the surface, which leave two electrons per vacancy in the Ti-t_{2g} orbitals. It is to be expected that some of this charge will be transferred to the FeSe, affecting the Fermi surface of the monolayer, although the amount is unclear *a priori*. To test this, we calculated the electronic structure of STO + FeSe with a 2DEG on the STO substrate.

In order to generate a 2DEG on STO without reducing the symmetry, we replaced 20% of the surface oxygen atoms with fluorine using the virtual crystal approximation. This leads

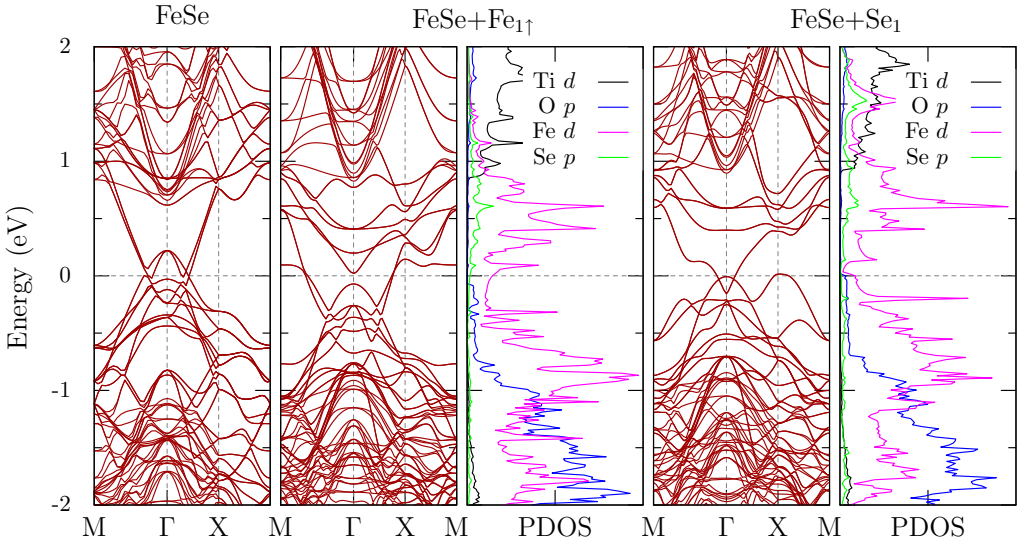

FIG. 3. (Color online) Non-spin-polarized band structures and density of states in the doubled unit cell of STO + FeSe (bare), with excess Fe and with excess Se in the lowest energy configurations. The doubling of the unit cell folds the electron and hole pockets to the zone center. Excess Fe is treated as magnetic.

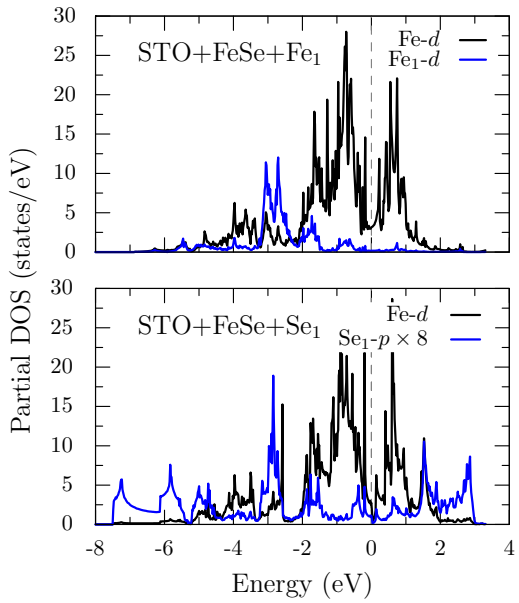

FIG. 4. (Color online) Partial density of states of the monolayer Fe-d and the excess Fe$_1$-d (top) and the excess Se$_1$-p (bottom). The Fermi level is set to 0.

to 0.4 electron per surface unit cell (there are two O per surface cell for TiO_2 termination), which corresponds to an electron density $n_e \sim 10^{20}$ cm^{-2} on the surface. Note that the actual 2DEG densities under the experimental conditions will depend on the number of oxygen vacancies and other defects generated during the surface preparation and FeSe deposition. As expected, these additional electrons reside in the Ti t_{2g} bands near the surface as shown in Fig. 5(a).

Next, using the relaxed structure with vdW interactions (with $d_S = 4.19$ Å), we calculated the band structure with

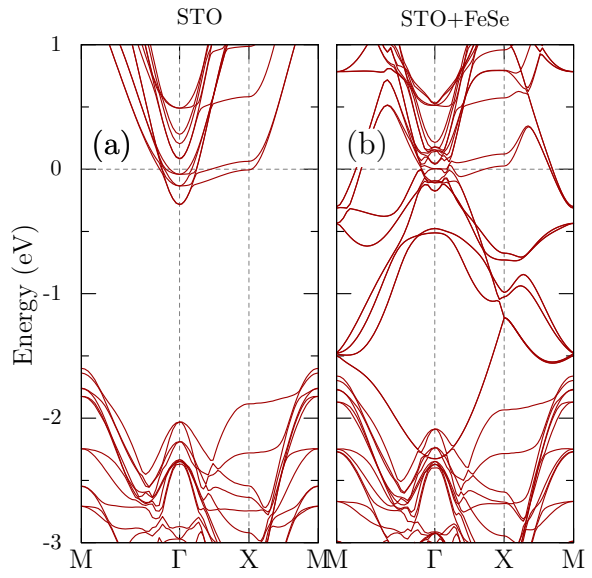

FIG. 5. (Color online) (a) Electronic structure of a bare STO slab with surface ($O_{1-x}F_x$) layers calculated within the virtual crystal approximation with $x = 0.2$, to simulate a 2DEG at the surface. (b) Band structure of the STO and FeSe monolayer system in the presence of a 2DEG on STO.

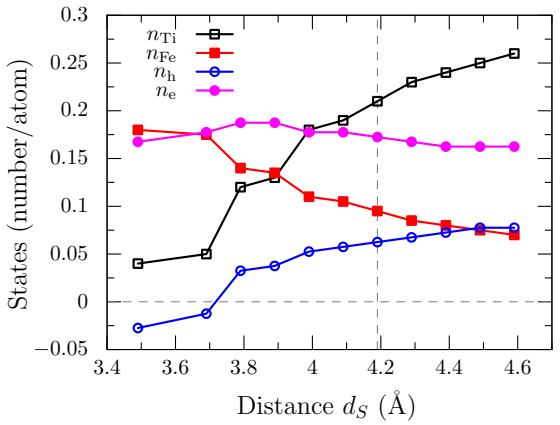

FIG. 6. (Color online) Charge transfer from STO to FeSe as a function of the distance between the two. n_{Ti} and n_{Fe} are the additional electrons in the Ti-t_{2g} and Fe-d states from oxygen vacancies and $n_{Ti} + 2n_{Fe} = 0.4$. n_e and n_h are the number of electrons in the pockets around the M and Γ points, respectively. The dashed vertical line corresponds to the vdW relaxed distance without charges. The hole states are completely removed below 3.8 Å.

a surface 2DEG, which is plotted in Fig. 5(b). Compared to Fig. 2, we find that the FeSe bands have shifted up by about 1 eV. Closely inspecting the bands around the Fermi level, we can see evidence of charge transfer from STO to the monolayer. Counting the states gives about 0.1 extra electron per Fe, reducing the surface 2DEG to 0.21 electron. However, the hole pockets around Γ are not fully removed since the pockets are 0.11 hole per Fe deep, and in addition, some of the transferred charge goes to the electron pocket around M. From the relative change in size of the two pockets we estimate that 0.07 electron goes to the hole pocket, which is not sufficient to fully remove it. Two scenarios that can potentially increase the electron doping of the FeSe monolayer are (a) a higher 2DEG density at the STO, which can transfer more charge to the monolayer, and (b) a reduced substrate-to-monolayer distance due to other interactions arising from other sources.

We estimated the effect of distance between STO and the monolayer on the charge transfer and the results are summarized in Fig. 6. We find that the charge transferred from the 2DEG to FeSe increases as the distance is reduced. Below a distance $d_S = 3.8$ Å, the hole states around the Γ point in the FeSe band structure are completely suppressed, while the electron pocket around M remains more or less unaffected. However, this requires an additional displacement of 0.4 Å of the monolayer towards the surface from the relaxed distance of $d_S = 4.19$ Å obtained in the previous section. The electrostatic attraction resulting from the charge transfer can potentially reduce d_S further, and analyzing the forces on the atoms we estimate this reduction to be about 0.1 Å.

IV. CONCLUSIONS

We have studied the effect of excess atoms and oxygen vacancies on the electronic structure of the STO + FeSe system with the help of first-principles calculations. We find that the vdW interactions play an important role in stabilizing the system. The excess atoms prefer the X_1 site above the

lower Se atoms, which allows them to bond strongly to the surface. The excess Fe atoms are magnetic, while the excess Se atoms bond strongly with the Fe of the monolayer. The oxygen vacancies induce a 2DEG on the STO surface which is partially transferred to the monolayer. Thus, we identify two mechanisms for electron doping of FeSe monolayers on STO: (1) O deficiency at the STO surface and (2) excess Fe. While excess Fe and Se defects are mutually exclusive, a reducing environment favors both excess Se and oxygen vacancies.

ACKNOWLEDGMENTS

This research was supported by the US Department of Energy, Basic Energy Sciences, Office of Science, Materials Sciences and Engineering Division.

[1] Y. Kamihara, T. Watanabe, M. Hirano, and H. Hosono, Iron-based layered superconductor $La[O_{1-x}F_x]FeAs(x = 0.05–0.12)$ with $T_c = 26$ K, J. Am. Chem. Soc. **130**, 3296 (2008).

[2] C. de la Cruz, Q. Huang, J. W. Lynn, J. Li, W. Ratcliff II, J. L. Zarestky, H. A. Mook, G. F. Chen, J. L. Luo, N. L. Wang, and P. Dai, Magnetic order close to superconductivity in the iron-based layered $LaO_{1-x}F_xFeAs$ systems, Nature **453**, 899 (2008).

[3] I. I. Mazin, D. J. Singh, M. D. Johannes, and M. H. Du, Unconventional superconductivity with a sign reversal in the order parameter of $LaFeAsO_{1-x}F_x$, Phys. Rev. Lett. **101**, 057003 (2008).

[4] D. C. Johnston, The puzzle of high temperature superconductivity in layered iron pnictides and chalcogenides, Adv. Phys. **59**, 803 (2010).

[5] D. J. Singh, Superconductivity and magnetism in 11-structure iron chalcogenides in relation to the iron pnictides, Sci. Technol. Adv. Mater. **13**, 054304 (2012).

[6] M. H. Fang, H. M. Pham, B. Qian, T. J. Liu, E. K. Vehstedt, Y. Liu, L. Spinu, and Z. Q. Mao, Superconductivity close to magnetic instability in $Fe(Se_{1-x}Te_x)_{0.82}$, Phys. Rev. B **78**, 224503 (2008).

[7] F.-C. Hsu, J.-Y. Luo, K.-W. Yeh, T.-K. Chen, T.-W. Huang, P. M. Wu, Y.-C. Lee, Y.-L. Huang, Y.-Y. Chu, D.-C. Yan, and M.-K. Wu, Superconductivity in the PbO-type structure α-FeSe, Proc. Natl. Acad. Sci. USA **105**, 14262 (2008).

[8] Y. Mizuguchi, F. Tomioka, S. Tsuda, T. Yamaguchi, and Y. Takano, Superconductivity at 27 K in tetragonal FeSe under high pressure, Appl. Phys. Lett. **93**, 152505 (2008).

[9] S. Medvedev, T. M. McQueen, I. A. Troyan, T. Palasyuk, M. I. Eremets, R. J. Cava, S. Naghavi, F. Casper, V. Ksenofontov, G. Wortmann, and C. Felser, Electronic and magnetic phase diagram of β-$Fe_{1.01}Se$ with superconductivity at 36.7 K under pressure, Nat. Mater. **8**, 630 (2009).

[10] Q.-Y. Wang, Z. Li, W.-H. Zhang, Z.-C. Zhang, J.-S. Zhang, W. Li, H. Ding, Y.-B. Ou, P. Deng, K. Chang *et al.*, Interface-induced high-temperature superconductivity in single unit-cell FeSe films on $SrTiO_3$, Chinese Phys. Lett. **29**, 037402 (2012).

[11] D. Liu, W. Zhang, D. Mou, J. He, Y.-B. Ou, Q.-Y. Wang, Z. Li, L. Wang, L. Zhao, S. He *et al.*, Electronic origin of high-temperature superconductivity in single-layer FeSe superconductor, Nature Commun. **3**, 931 (2012).

[12] S. He, J. He, W. Zhang, L. Zhao, D. Liu, X. Liu, D. Mou, Y.-B. Ou, Q.-Y. Wang, Z. Li *et al.*, Phase diagram and electronic indication of high-temperature superconductivity at 65 K in single-layer FeSe films, Nat. Mater. **12**, 605 (2013).

[13] S. Tan, Y. Zhang, M. Xia, Z. Ye, F. Chen, X. Xie, R. Peng, D. Xu, Q. Fan, H. Xu *et al.*, Interface-induced superconductivity and strain-dependent spin density waves in FeSe/$SrTiO_3$ Å thin films, Nat. Mater. **12**, 634 (2013).

[14] J. J. Lee, F. T. Schmitt, R. G. Moore, S. Johnston, Y.-T. Cui, W. Li, M. Yi, Z. K. Liu, M. Hashimoto, Y. Zhang *et al.*, Interfacial mode coupling as the origin of the enhancement of T_c in FeSe films on $SrTiO_3$, Nature **515**, 245 (2014).

[15] R. Peng, X. P. Shen, X. Xie, H. C. Xu, S. Y. Tan, M. Xia, T. Zhang, H. Y. Cao, X. G. Gong, J. P. Hu *et al.*, Measurement of an enhanced superconducting phase and a pronounced anisotropy of the energy gap of a strained FeSe single layer in FeSe:Nb:$SrTiO_3$/$KTaO_3$ heterostructures using photoemission spectroscopy, Phys. Rev. Lett. **112**, 107001 (2014).

[16] X. Liu, D.a Liu, W. Zhang, J. He, L. Zhao, S. He, D. Mou, F. Li, C. Tang, Z. Li *et al.*, Dichotomy of the electronic structure and superconductivity between single-layer and double-layer FeSe/$SrTiO_3$ films, Nature Commun. **5**, 5047 (2014).

[17] C.-L. Song, Y.-L. Wang, Y.-P. Jiang, Z. Li, L. Wang, K. He, X. Chen, X.-C. Ma, and Q.-K. Xue, Molecular-beam epitaxy and robust superconductivity of stoichiometric FeSe crystalline films on bilayer graphene, Phys. Rev. B **84**, 020503 (2011).

[18] Z. Li, J.-P. Peng, H.i-M.n Zhang, W.-H. Zhang, H. Ding, P. Deng, K. Chang, C.-L. Song, S.-H. Ji, L. Wang *et al.*, Molecular beam epitaxy growth and post-growth annealing of FeSe films on $SrTiO_3$: A scanning tunneling microscopy study, J. Phys.: Condens. Matter **26**, 265002 (2014).

[19] J. He, X. Liu, W. Zhang, L. Zhao, D. Liu, S. He, D. Mou, F. Li, C. Tang, Z. *et al.*, Electronic evidence of an insulator-superconductor crossover in single-layer FeSe/$SrTiO_3$ films, Proc. Natl. Acad. Sci. USA **111**, 18501 (2014).

[20] J. Bang, Z. Li, Y. Y. Sun, A. Samanta, Y. Y. Zhang, W. Zhang, L. Wang, X. Chen, X. Ma, Q.-K. Xue, and S. B. Zhang, Atomic and electronic structures of single-layer FeSe on $SrTiO_3$(001): The role of oxygen deficiency, Phys. Rev. B **87**, 220503 (2013).

[21] T. Bazhirov and M. L Cohen, Effects of charge doping and constrained magnetization on the electronic structure of an FeSe monolayer, J. Phys.: Condens. Matter **25**, 105506 (2013).

[22] F. Zheng, Z. Wang, W. Kang, and P. Zhang, Antiferromagnetic FeSe monolayer on $SrTiO_3$: The charge doping and electric field effects, Sci. Rep. **3**, 2213 (2013).

[23] T. Berlijn, H.-P. Cheng, P. J. Hirschfeld, and W. Ku, Doping effects of Se vacancies in monolayer FeSe, Phys. Rev. B **89**, 020501 (2014).

[24] W. Zhang, Z. Li, F. Li, H. Zhang, J. Peng, C. Tang, Q. Wang, K. He, X. Chen, L. Wang *et al.*, Interface charge doping effects on superconductivity of single-unit-cell FeSe films on $SrTiO_3$ substrates, Phys. Rev. B **89**, 060506 (2014).

[25] J. N. Eckstein, Oxide interfaces: Watch out for the lack of oxygen, Nat. Mater. **6**, 473 (2007).

[26] G. Kresse and J. Hafner, Ab initio molecular dynamics for liquid metals, Phys. Rev. B **47**, 558 (1993); G. Kresse and J. Furthmüller, Efficient iterative schemes for *ab initio* total-energy calculations using a plane-wave basis set, *ibid.* **54**, 11169 (1996).

[27] P. E. Blöchl, Projector augmented-wave method, Phys. Rev. B **50**, 17953 (1994).

[28] J. P. Perdew, K. Burke, and M. Ernzerhof, Generalized gradient approximation made simple, Phys. Rev. Lett. **77**, 3865 (1996).

[29] S. Grimme, J. Antony, S. Ehrlich, and H. Krieg, A consistent and accurate ab initio parametrization of density functional dispersion correction (DFT-D) for the 94 elements H-Pu, J. Chem. Phys. **132**, 154104 (2010); S. Grimme, S. Ehrlich, and L. Goerigk, Effect of the damping function in dispersion corrected density functional theory, J. Comp. Chem. **32**, 1456 (2011).

[30] K. Liu, Z.-Y. Lu, and T. Xiang, Atomic and electronic structures of fese monolayer and bilayer thin films on $SrTiO_3$ (001): First-principles study, Phys. Rev. B **85**, 235123 (2012).

[31] A. Subedi, L. Zhang, D. J. Singh, and M. H. Du, Density functional study of FeS, FeSe, and FeTe: Electronic structure, magnetism, phonons, and superconductivity, Phys. Rev. B **78**, 134514 (2008).

[32] L. Zhang, D. J. Singh, and M. H. Du, Density functional study of excess Fe in $Fe_{1+x}Te$: Magnetism and doping, Phys. Rev. B **79**, 012506 (2009).